Regime Shift to Hyperturbid Conditions in the Loire Estuary
Overview of Observations and Model Analysis of Physical Mechanisms

Dijkstra, Yoeri M.; de Goede, Roel J.A.

DOI
10.1029/2023JC020273

Publication date
2024

Document Version
Final published version

Published in
Journal of Geophysical Research: Oceans

Citation (APA)
Dijkstra, Y. M., & de Goede, R. J. A. (2024). Regime Shift to Hyperturbid Conditions in the Loire Estuary: Overview of Observations and Model Analysis of Physical Mechanisms. *Journal of Geophysical Research: Oceans*, *129*(9), Article e2023JC020273. https://doi.org/10.1029/2023JC020273

ADVANCING EARTH AND SPACE SCIENCES

JGR Oceans

RESEARCH ARTICLE

10.1029/2023JC020273

Key Points:

- A review of observations from 1950 to 2013 reveals a dramatic increase, or regime shift, in sediment concentrations in the Loire estuary
- Using an idealized model, the observed regime shift is qualitatively reproduced and attributed to deepening of the estuary
- The dominant transport processes causing the regime shift are related to gravitational circulation and tidal asymmetry originating at sea

Supporting Information:

Supporting Information may be found in the online version of this article.

Correspondence to:

Y. M. Dijkstra,
y.m.dijkstra@tudelft.nl

Citation:

Dijkstra, Y. M., & de Goede, R. J. A. (2024). Regime shift to hyperturbid conditions in the Loire estuary: Overview of observations and model analysis of physical mechanisms. *Journal of Geophysical Research: Oceans*, *129*, e2023JC020273. https://doi.org/10.1029/2023JC020273

Received 28 JUL 2023
Accepted 6 SEP 2024

Author Contributions:

Conceptualization: Yoeri M. Dijkstra, Roel J. A. de Goede
Data curation: Yoeri M. Dijkstra
Formal analysis: Yoeri M. Dijkstra, Roel J. A. de Goede
Investigation: Yoeri M. Dijkstra, Roel J. A. de Goede
Methodology: Yoeri M. Dijkstra
Software: Yoeri M. Dijkstra
Supervision: Yoeri M. Dijkstra
Validation: Yoeri M. Dijkstra, Roel J. A. de Goede
Visualization: Yoeri M. Dijkstra
Writing – original draft: Yoeri M. Dijkstra, Roel J. A. de Goede

Regime Shift to Hyperturbid Conditions in the Loire Estuary: Overview of Observations and Model Analysis of Physical Mechanisms

Yoeri M. Dijkstra[1] and Roel J. A. de Goede[2]

[1]Delft Institute of Applied Mathematics, Delft University of Technology, Delft, The Netherlands, [2]Deltares, Marine and Coastal Systems Unit, Delft, The Netherlands

Abstract The Loire estuary (France) was extensively deepened during the 20th century. Coincidentally, suspended sediment concentrations increased drastically from ∼0.1 g/l to ∼1–5 g/l at the surface and the estuarine turbidity maximum (ETM) moved upstream. In this study we, for the first time, brought together a century of observations of estuary bed level, tidal amplitude, and sediment concentration to demonstrate these large changes. Next, we analyzed a minimal set of physical mechanisms that explain the dramatic increase in sediment concentration. To this end, we used the iFlow model representing dynamic equilibrium conditions in the Loire. Novel in the model is that it dynamically resolves salt stratification and corresponding damping of turbulence. For conditions representing the year 2000, high sediment concentrations were found with satisfactory correspondence to observations. Low sediment concentrations were found when using the year 1900 bed level but keeping all other model parameters the same. Varying the bed level gradually between these two extremes, the equilibrium solution suddenly increases for intermediate bed level, constituting an abrupt regime shift. Robustness of this result was established in an extensive sensitivity study featuring 13,200 model experiments. The regime shift is enabled by a feedback between increasing sediment concentration, reducing turbulence due to sediment and salt stratification, and increasing sediment importing capacity of the estuary. The essential sediment importing mechanisms in this feedback are related to the tidal asymmetry and gravitational circulation. This is the first time gravitational circulation and salt stratification are shown to be important factors in a transition to hyperturbidity.

Plain Language Summary Over the course of the 20th century, the Loire River estuary in France was deepened to allow for shipping and for mining of sand. At the same time, suspended sediment concentrations have increased over a factor 10, with destructive impact on the ecosystem. In this study we firstly brought together several decades of field observations to demonstrate these large changes. Secondly, we investigated which physical processes are responsible for the observed increase in sediment concentration. This was done using an idealized model that includes a selection of essential physical processes and allows for in-depth analysis. It was found these processes are related to tidal asymmetry and to flows driven by density differences between fresh and salt water. Using the model we also found so called tipping-point behavior: the estuary suddenly supports a much larger sediment concentration after a certain bed level threshold is exceeded. From a study involving 13,200 model experiments for different parameter values we found that these results are robust to uncertainty in parameter values. Finally, we placed the results in context of other estuaries.

1. Introduction

Human interference in estuaries, such as deepening, training of shipping channels, or reduction in fresh water supply, can sometimes have extreme consequences on the water motion and sediment dynamics. Winterwerp and Wang (2013) hypothesized that, in some estuaries, human-induced deepening can cause a *regime shift*, where sediment concentrations increase by orders of magnitude from ∼0.1 g/l to concentrations of ∼10 g/l or more, that is, a hyperturbid state. There is strong evidence that such a regime shift has occurred in the Ems estuary (Germany) (De Jonge et al., 2014). It is suggested that a similar regime shift occurred in the Loire estuary (France) (Winterwerp et al., 2013). However, direct evidence of this regime shift by comparing historical and present-day observations of sediment concentrations is still missing. In both the Loire and Ems, the present-day high sediment concentrations led to hypoxic zones with destructive effects on local ecosystems (Schmidt et al., 2019; Talke et al., 2009). It is important to learn as much as possible about the mechanisms causing the transition to

10.1029/2023JC020273

Writing – review & editing: Yoeri M. Dijkstra, Roel J. A. de Goede

hyperturbidity to understand if other estuaries are facing a similar threat and to assist in the design of mitigating measures.

There is a large body of literature discussing mechanisms trapping sediments, related to for example, density driven flow (e.g., Burchard & Baumert, 1998; Festa & Hansen, 1978; Geyer, 1993; Scully & Friedrichs, 2007) and tidal flow (e.g., Allen et al., 1980; Chernetsky et al., 2010). We refer to Burchard et al. (2018) for a more comprehensive overview. Several of these processes have been linked to regime shift to hyperturbid conditions. Winterwerp and Wang (2013) and Van Maren et al. (2015) introduced the first theory of how deepening may lead to a dramatically increased sediment trapping. They argued that deepening can alter the tidal motion, leading to faster and shorter flood currents and prolonged HW slack periods (meaning relatively much settling of sediment during slack and hence low concentrations at the start of ebb). These changes increase sediment import from the adjacent sea. This leads to an elevated sediment concentration, which reduces turbulent mixing in the estuary, further altering the tidal motion in a way that increases sediment import. They hypothesized this leads to a positive feedback loop resulting in extremely high sediment concentrations. Dijkstra, Schuttelaars, Schramkowski, & Brouwer (2019) demonstrated the existence of this positive feedback mechanism using an idealized process-based model and qualitatively reproduced the regime shift observed in the Ems. They also made several refinements to the theory. Firstly, they showed that deepening and reduction of turbulence in the Ems had relatively little effect on the M_2 tidal velocity but instead greatly amplified the M_4 velocity, which increased the tidal asymmetry. They argued this happened because deepening and reduction of turbulence brought the estuary closer to a resonating state for the M_4 tide. Secondly, the mechanism required both a sediment-induced reduction to the turbulent mixing in the water column as well as sediment-induced reduction of the bottom form drag.

Besides tidal asymmetry, it is not unlikely that estuarine exchange flow plays a role as well. Although there is no evidence of a regime shift to hyperturbidity caused dominantly by exchange flows, Van Maren et al. (2020) found that a similar feedback between the exchange flow and sediment-induced reduction of turbulence is able to maintain somewhat elevated sediment concentrations (~ 100 mg/l) in the Belgian coastal zone. Additionally, once sediment concentrations reach appreciably high levels, it has been observed that tidally asymmetric stratification and entrainment of mud is capable of maintaining high levels of sediment trapping, reinforcing and sustaining the hyperturbid conditions (Becker et al., 2018; Winterwerp et al., 2017). Lin et al. (2021) emphasize that a regime shift does not only occur in the along-channel sediment distribution but also in vertical stratification. As the amount of sediment in a water column increases, reduced turbulence causes rapidly increasing sediment stratification with high concentrations near the bed (e.g., Ge et al., 2018; Winterwerp, 2001) kept in suspension by hindered settling (Dijkstra et al., 2018; Manning et al., 2010). This self-reinforcing process is thought to create stable pools of mud that are not easily flushed from the estuary during high discharge events (Winterwerp et al., 2017).

Not every estuary seems susceptible to a similar regime shift to hyperturbidity as a result of deepening. At the moment, there is no general theory describing which estuaries are and are not susceptible to a regime shift, and we need to rely on lessons learned from studies of individual estuaries.

As a step toward a more general theory, the goal of this study is to identify physical mechanisms that may have caused the regime shift to a hyperturbid state in the Loire estuary. To this end, we first reviewed relevant historical observations to find direct evidence that a regime shift indeed occurred and describe the sediment distribution. A review of such data or even a study that establishes the observation of a regime shift seems to be missing entirely. While the water motion, sediment concentrations, and settling velocity in recent decades were measured at high resolution (Jalón-Rojas et al., 2016; Sogreah, 2010), historical data is scarce scattered over technical reports. Next, we followed a similar methodology as Dijkstra, Schuttelaars, Schramkowski, and Brouwer (2019), using the idealized width-averaged iFlow model to qualitatively reproduce the regime shift and systematically analyze the underlying processes. The model was calibrated to a recent state and computed back in time, comparing to the available historic observations. Here we explicitly used the unique advantage of iFlow over more realistic and complex models: its ability to run using little calibration data and conduct extensive sensitivity analysis to cope with the large uncertainty resulting from the lack of observations. Hence, we argue that we can draw robust conclusions despite the large uncertainty.

The review of available observations as well as the model set-up are presented in Section 2. We next show the model results, in comparison with observations, for a default case representing summer (i.e., low) discharge conditions in the Loire in Section 3. The sensitivity of the results to parameters is presented in Section 4, first focusing on higher discharges and next showing the effect of variations and uncertainty in various model parameters. Section 5 discusses the limitations of this work and discusses the comparison to the Ems estuary and implications for other estuaries. Finally, the main novel findings of this work are summarized in Section 6.

2. Model Approach and Observations

2.1. Model Description

We used the iFlow model (v3.1), which extends the models used by Dijkstra, Schuttelaars, Schramkowski, and Brouwer (2019), Dijkstra et al. (2019a). This model resolves the width-averaged tidal and subtidal water motion and sediment dynamics. New compared the studies mentioned above, the model explicitly resolves the subtidal salinity and salt stratification. We summarize the main features of the model here and refer to Dijkstra, Brouwer, et al. (2017), Dijkstra, Schuttelaars, Schramkowski, and Brouwer (2019) for details. Details of the new salinity module are included in the Supporting Information S1.

In the iFlow model, the geometry of an estuary is described by a rectangular cross-section. The width B and bed level $-H$ vary in the along-channel direction. The profiles of B and H are based on observations which were smoothed to remove topographic variations on short length scales but represent estuary-scale (i.e., ∼10 km) variations. The water motion is consequently solved using the width-averaged continuity and momentum equations:

$$(Bu)_x + Bw_z = 0, \tag{1}$$

$$u_t + uu_x + wu_z = -g\zeta_x + g\beta\int_z^{\zeta} s_x\, dz' + \left(A_\nu u_z\right)_z, \tag{2}$$

where u and w are the velocity in the along-channel direction ($0 < x < L$) and vertical direction ($-H < z < \zeta$), ζ is the free surface elevation, s is salinity, g is the acceleration of gravity, β is the haline contraction coefficient ($7.6 \cdot 10^{-4}$ psu^{-1}), and A_ν is the vertical eddy viscosity. The boundary conditions are given by kinematic and no-stress surface conditions and a no-flux and partial slip bottom boundary condition. Specifically, the partial slip condition reads as $A_\nu u_z = s_f u$, where s_f is the bottom friction coefficient. At the downstream boundary ($x = 0$), the model is forced by a reduced tidal signal, consisting of a semi-diurnal (hereafter D_2) and quarter-diurnal (hereafter D_4) tide. The D_2 tide represents the combination of the M_2, S_2 and all other semi-diurnal constituent tides at either spring tide or neap tide (see Section 2.2 for precise definitions). Similarly, the D_4 tide represents the combination of all quarter-diurnal constituents. At the upstream boundary ($x = L$), a constant river discharge is applied. Salinity is assumed well-mixed in the vertical and gradually varying in the along-channel direction according to a prescribed function that fits observations (see Section 2.2). The above equations are solved using a perturbation approach, assuming the water level elevation is small compared to the depth, bathymetric variations are on the estuary scale (∼10 km), and density-driven flow, D_4 tide, and river-induced flows are much smaller than the D_2 tidal flow.

Sediment concentration c is modeled using a single suspended sediment fraction assuming constant settling velocity w_s, which is reduced by the effects of hindered settling according to a modification of the relation by Richardson and Zaki (1954)

$$w_s = w_{s,0}\left\langle \left(1 - \frac{c_{\text{bed}}}{c_{\text{gel}}}\right)^5 \right\rangle, \tag{3}$$

where $w_{s,0}$ is the clear-water settling velocity, c_{bed} is the sediment concentration near the bed, c_{gel} is the gelling concentration, and $\langle\cdot\rangle$ denotes tidal averaging. This expression implies that the settling velocity remains constant in time, uniform in the vertical, but varying along the channel. The tidal and subtidal sediment motion is resolved using a mass conservation equation:

$$c_t + uc_x + (w - w_s)\, c_z = \left(K_\nu c_z\right)_z + \frac{1}{B}(BK_h c_x)_x, \tag{4}$$

where K_ν and K_h are the vertical and horizontal eddy diffusivity. The sediment equation is subject to a no-flux condition at the surface, and sediment is allowed to deposit and erode from the bed. The erosion rate E is modeled using a simplified Partheniades relation, not accounting for critical shear stress:

$$E = M|\tau_b|f = M|s_s u_{-H}|f. \tag{5}$$

Here M is an empirical erosion parameter, s_s is a bottom friction coefficient for sediment erosion (see below), and f is the tidally averaged sediment erodibility. The erodibility is a number between zero and one indicating the tidally averaged availability erodible sediment on the bed from no sediment ($f = 0$) to abundant sediment ($f = 1$) (Brouwer et al., 2018). At the seaward boundary, the sediment model is forced by prescribing the tide-and-depth averaged component of the concentration c_{sea}. At the landward boundary, a zero sediment inflow is prescribed (cf. Section 2.2). Like the hydrodynamic model, the sediment model is solved using a perturbation approach. This approach leads to linear equations at each order, so that the effects of various physical processes may be studied in isolation. Notably, this allows decomposition of the sediment transport balance into various physical contributions, listed and explained in Section 3.4.

Salinity is considered to be fully governed by subtidal processes and is resolved using the model of MacCready (2004). This model captures salt transport by gravitational circulation and by dispersion parametrized by a dispersion coefficient $K_{h,\text{sal}}$. The model also resolves salt stratification. The full model is described in the online supplement.

The effects of turbulence are parametrized using an eddy viscosity A_ν, eddy diffusivity K_ν and linearized bed shear stress coefficients s_f and s_s. The eddy viscosity and eddy diffusivity are assumed constant over the tidal cycle and in the vertical but variable along the channel. The value of the eddy viscosity is a function of the local velocity amplitude, depth and salt and sediment stratification, thus accounting for density-induced damping of turbulence, according to

$$A_\nu = \left\langle c_{\nu,1}\left(z_0^*\right)|U|(H+\zeta)F\left(\overline{\text{Ri}}\right)\right\rangle, \tag{6}$$

$$K_\nu = \left\langle \frac{c_{\nu,1}\left(z_0^*\right)}{\sigma_\rho}|U|(H+\zeta)G\left(\overline{\text{Ri}}\right)\right\rangle. \tag{7}$$

Here, $c_{\nu,1}\left(z_0^*\right)$ is a coefficient that depends on a calibrated dimensionless roughness height z_0^*, $|U|$ is the tide-and-depth-averaged velocity magnitude, and $F\left(\overline{\text{Ri}}\right)$, $G\left(\overline{\text{Ri}}\right)$ are adaptations of the Munk and Anderson (1948) functions for stratification-induced damping of turbulence. They depend on the depth-average $(\bar{\cdot})$ of an approximation of the Richardson number

$$\text{Ri} == -g\,\frac{\beta_c c_z + \beta s_z}{u_z^2 + u_{z,\min}^2}. \tag{8}$$

Here $u_{z,\min} = 0.03\ \text{s}^{-1}$ parametrizes the unresolved shear, for example, by lateral flows and $\beta_c = 6.2 \cdot 10^{-4}\ \text{m}^3/\text{kg}$. This definition of the Richardson number accounts for both salt- and sediment-induced stratification. Stratification by temperature is neglected. The damping functions F and G read as

$$F\left(\overline{\text{Ri}}\right) = \left(1 + 10\overline{Ri}\right)^{-1/2}, \tag{9}$$

$$G\left(\overline{\text{Ri}}\right) = \left(1 + 3.33\overline{Ri}\right)^{-3/2}. \tag{10}$$

Furthermore, the bed stress coefficient for sediment s_s parametrizes stress at the bed and is assumed a function of U. The bed stress coefficient for the water motion s_f additionally parametrizes the form drag created by dunes and ripples on the bed and possible sediment stratification occurring close to the bed. Hence, s_f is assumed a function of U as well as the near-bed sediment stratification. As the salinity gradient vanishes near the bed, it has no effect on s_f.

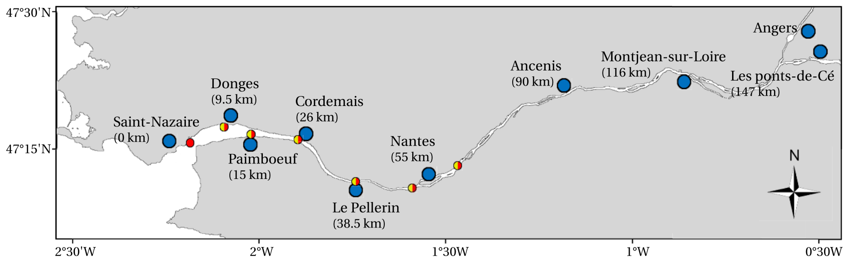

Figure 1. Map of the Loire estuary (France) from Saint-Nazaire to Les ponts-de-Cé. The bigger blue circles indicate several towns along the estuary. Smaller dots indicate locations of tidal gauges (red) and measurement stations of the SYVEL network (yellow), measuring various quantities including salinity and turbidity (www.loire-estuaire.org).

The effects of wind waves is not explicitly taken into account in this study. It is estimated that wind waves are especially important on shallow lateral flanks that are not explicitly resolved in this width-averaged model. Effects of waves on the width-averaged circulation and resuspension of sediment is parametrically included in the parameters K_h and M, respectively.

The model is solved assuming dynamic equilibrium, that is, the state obtained after a long time of constant tidal and subtidal forcing. The main advantage of this approach, is that the tidally averaged sediment balance is exactly closed, so we may regard it as a precise balance independent of time. Furthermore, by solving the model for dynamic equilibrium directly, no time stepping procedure is required, greatly reducing computation time in comparison to time-stepping models.

2.2. The Loire: Geometry and Water Motion

The Loire is a 1,012 km long river in France. We considered the Loire estuary from the mouth at Saint-Nazaire (0 km) to Les Ponts-de-Cé (km 147), well beyond the tidal limit (see Figure 1). For the estuary width, we considered the width of the channel in such a way that the cross-sectional area matches observations. The resulting width converges from roughly 1 km at the mouth to 250 m at Nantes (km 55). The most significant interventions that changed the width of the main channel date back to before 1915 (Sogreah, 2006). Since we focussed on the period from roughly 1900 to 2000, we assume channel width is constant over time in this study.

Bed level: we assumed the representative bed level equals the thalweg level, for which observations are available from 2009, for simplicity called the year 2000 bed, d_{2000} (GIP, 2014), as well as around the year 1900, for simplicity referred to as the year 1900 bed, d_{1900} (GIP, 2004; GIP, 2011). The data is plotted in Figure 2. The figure also shows data of the thalweg level used by Le Hir (1994) (see also Rosales-Sierra & Levacher, 2004) and the threshold bed levels specified by dredging operations as summarized in Table 1 for before 1948 and before 1973 (Sogreah, 2006). The solid lines in the figure represent the smooth fits used in our model study to represent bed levels in 1900 and 2000. Plotted bed-levels are approximately with respect to mean sea level in the year 2009. Between 1900 and 2009, mean sea level has increased by approximately 13 cm (Ferret, 2016). The sea level rise is

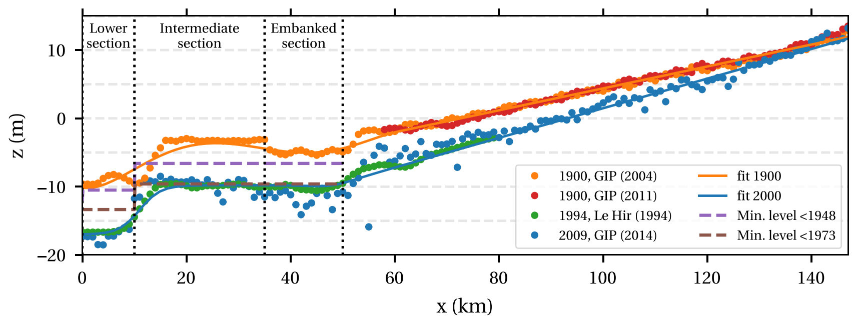

Figure 2. Thalweg level of the Loire upstream from Saint-Nazaire. Data is presented from between 1900 and 2009 (GIP, 2004, 2011, 2014; Le Hir, 1994). Additionally, the solid lines show the smooth fits used in the model for the 1900 and 2000 cases. Dashed lines show data of threshold bed levels specified by dredging operations (see Table 1, Sogreah (2006)).

10.1029/2023JC020273

Table 1
Interventions in the Loire Downstream of Nantes (Sogreah, 2006)

Year	Intervention
1898–1899	Embanked section (km 37–52) dredged to CM96[a] −1.2 m.
1906–1912	Intermediate channel (km 10–37) deepened from CM96 + 0.9 m to −2.1 m.
1913–1920	Creation of "Bassin de Marée" upstream of Nantes.
1940	Lower section (km 0–10) deepened to CM96–6.5 m.
1942	Exterior section (< km 0) deepened to CM96 -8 m.
1948–1968	Intermediate and embanked sections (km 10–52) deepened from CM96–2.6–5.1 m.
1969–1973	Exterior section deepened to CM96–9.4 m. Lower section (km 0–10) deepened to CM96–9.35. Intermediate and embanked sections (km 10–52) deepened to CM96–5.6 m.
1978–1980	Exterior and lower sections (km 0–10) deepened to CM96–12.85 m.
1985–1986	Exterior section deepened to CM96–13.7 m

[a]CM96 is the local chart datum, approximately 3.6 m below MSL at Saint-Nazaire (Jalón-Rojas et al., 2016).

a relatively small change compared to the deepening of over 5 m in the first 50 km and is not taken into account in our study.

Over the century, the bed level was lowered by approximately 5 m over a significant part of the estuary. Here we note that much of this deepening in the intermediate and embanked sections (km 10–50) happened before the 1970s. Human interventions have played a large role in this. Besides dredging operations downstream of Nantes as summarized in Table 1, extensive sand mining in the main channel upstream of Nantes happened until 1992 and led to a bed degradation of up to 3 m (Briere et al., 2011; Gasowski, 1994). Natural morphological effects may additionally play a role in changing bed levels or redistributing the effects of local dredging operations. Apart from d_{1900} and d_{2000} we define d_α as a linear interpolation between the 1900 and 2000 bed level as

$$d_\alpha(x) = (1-\alpha)d_{1900}(x) + \alpha d_{2000}(x), \tag{11}$$

where α is a linear interpolation parameter that ranges between 0 and 1. We assumed for simplicity that each year between 1900 and 2000 may be associated with some value of α. While this may not be completely accurate, this is sufficient for the purposes of this study.

Discharge: the river discharge in the Loire in the period 2007–2013 at the station of Montjean-sur-Loire (km 116) had a yearly average of 910 m^3/s, a summer average (Jul–Oct.) of 300 m^3/s and a winter average (Jan–Mar.) of 1,300 m^3/s. Work by DREAL (2019) shows the overall discharge distribution has not changed significantly since at least 1863.

Tides: the tidal amplitude in the Loire depends on the season and varies over the spring-neap cycle. We analyzed the tidal amplitude based on 5-min resolution data at 7 stations (see red dots in Figure 1) over the period 2007–2014 (Jalón-Rojas et al., 2016). Tidal amplitudes were filtered from the signal using complex demodulation. This method was used to identify the subtidal, semi-diurnal and quarter-diurnal components, where the spring-neap cycle appears as a gradual variation of the semi-diurnal amplitude over a fortnightly period. We defined average spring (neap) tide as the median of the highest (lowest) 40% of the tides. The resulting amplitudes are shown in Figures 3a and 3b. Clearly, semi-diurnal spring tidal amplitudes are around 80% larger than neap tidal amplitudes. Also, tides are more strongly amplified in summer than winter, related possibly to tide-river interaction and varying amounts of salt and sediment stratification during winter and summer. Quarter-diurnal tides however are fairly insensitive to the seasons and the spring-neap cycle.

Figure 3c shows historical tidal data which are all for spring tide during low discharge conditions. The observations clearly show an increase in tidal amplitude over time, as also reported by Winterwerp et al. (2013).

Salinity: salinity was compared to the salinity in the calibrated three-dimensional model of Grasso and Caillaud (2023). Model data was chosen here over observations, because it provides better along-channel coverage at consistent vertical levels and always along the thalweg, and also simply because pre-processed model data was

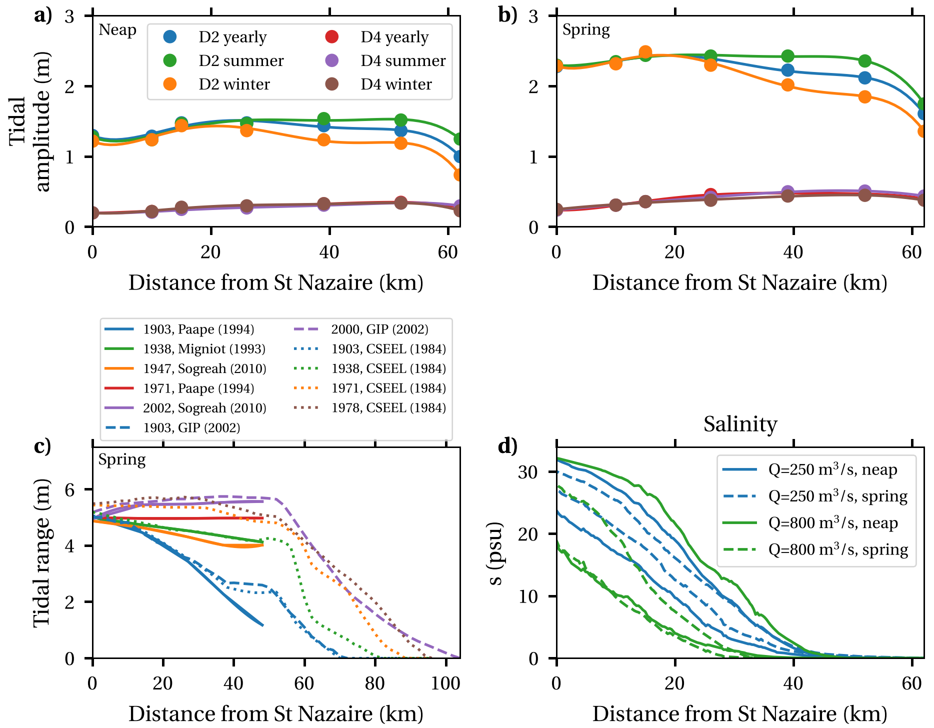

Figure 3. (a–b) Observed tidal amplitudes filtered from tidal gauge measurements using complex demodulation (Jalón-Rojas et al., 2016). (c) tidal range during low discharge and spring tide over the 20th century (GIP, 2002; Migniot, 1993; Paape, 1994; Sogreah, 2010). (d) 2008–2018 3D modeled average salinity in the thalweg for two discharge classes and spring and neap conditions. For each conditions, two lines are plotted representing surface and bottom salinity.

readily available. Grasso and Caillaud (2023) show reasonable correspondence between model and observations over the various seasons, so that the model data is sufficiently accurate for the purposes of this study. The salinity from the 3D model was averaged over the modeling period from 2008 to 2018 in the thalweg grouped by various discharge classes (<200, 200–300, 300–600, 600–850, >850 m^3/s) and by spring and neap tidal conditions. Surface and bed values for two discharge classes and spring and neap conditions are shown in Figure 3d for illustration. These data clearly show a much stronger salinity stratification during neap tide compared to spring tide due to less tidal mixing.

2.3. Historical and Present Observations of Sediment Concentrations

Probably the first investigator of turbidity in the Loire estuary was Leopold Berthois around 1950 (Guilcher, 1988). Measurements of Berthois and Barbier (1953); Berthois (1954, 1955) show that the turbid zone could be found up to Le Pellerin (km 39) with its maximum slightly downstream of Cordemais (km 26) in 1952 during spring tide and low river discharge, as shown in Figure 4. Averaged over a tidal cycle, concentrations in the ETM were around 0.25 g/l (surface) and 1 g/l (bed). Although most of the instantaneous concentrations reported at the time do not exceed 3 g/l (bed), Berthois (1955) mentions record of a maximum concentration near Cordemais of 20.5 g/l during summer, and Berthois (1957) reports concentrations of 5–15 g/l near the bed at the mouth. Unfortunately, no further clarification is provided, but it shows that high sediment concentrations could already occur in the 1950s.

Gallenne (1974a, 1974b) shows that the typical concentrations remain unchanged with values around 0.2–0.3 g/l (surface) in the 1970s compared to the 1950s. The turbid zone is reported to reach up to Nantes (km 52) for low discharge conditions, with the center of the ETM between Cordemais and Le Pellerin throughout the summer (km 26–39) (Gallenne, 1974b). Comparable concentrations were found by Saliot et al. (1984) and Rincé et al. (1989). According to Migniot (1993) and Paape (1994), tidally averaged concentrations near the surface in the range 0.3–0.7 g/l were common in the early 1990s. The turbid zone also extended further inland and reached up to km 60.

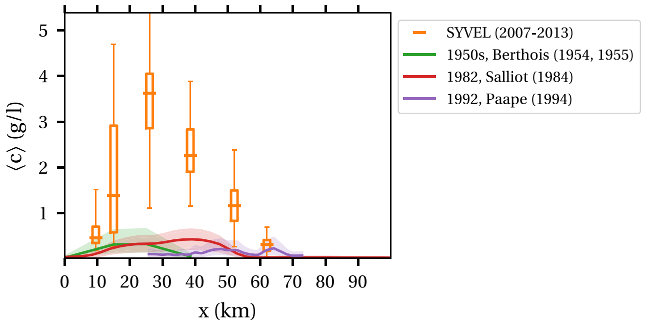

Figure 4. Evolution of the tidally averaged sediment concentration $\langle c \rangle$ near the water surface for low river discharges and spring tidal conditions since the 1950s. The green curve is an estimate of tidally averaged concentrations in the 1950s from instantaneous measurements (Berthois, 1954, 1955). The shaded area is used to indicate the observed spread. The most recent turbidity measurements are from the SYVEL network (Jalón-Rojas et al., 2016).

Jalón-Rojas et al. (2016) track the movement of the ETM in the period 2007–2013 using data from the SYVEL network. They show that the ETM is found between km 25–40 for low discharges (<200 m^3/s) with near-surface concentrations of 3 g/l on average during spring tide and 1 g/l on average during neap tide. Model studies by Normant (2000) and Sogreah (2010) show that corresponding near bed concentrations should be of the order of 10–20 g/l.

Even though we could not find records of high surface concentrations in the 1970s–1990s as observed more recently, both Gallenne (1974a) and CSEEL (1984) discuss the existence of extensive fluid mud in the estuary in the 1970s and 1980s. This fluid mud was mixed up during peak ebb and flood, especially during spring tide. Gallenne (1974a) shows the fluid mud zone migrates between Donges (km 10) in winter and Le Pellerin (km 39) in summer in 1972 and is about 1 m thick. CSEEL (1984) report observing fluid mud of up to 2–3 m thick over a length of 20 km during slack tide and low discharge conditions in 1976. CSEEL (1984) also compare their observations from 1974 to 1976 and 1981, stating that there was a clearly observable movement of sandy material and sand dunes in 1974–1976 which was almost completely replaced by a muddy bed in 1981, even though they measured in the same seasons. Furthermore, they describe that the amount of mud in the estuary increased by 50% in 1981 compared to 1974.

Sediment concentrations at sea: in order to set a boundary condition for the sediment at the seaward boundary in the model, we look closer at the turbidity at the mouth of the Loire. Berthois (1955) showed that the sediment concentrations are in the order of 0.1–0.2 g/l for winter conditions, more or less uniformly distributed over the depth. During summer conditions, surface concentrations can fall by a factor 10 while concentrations near the bottom remain unchanged. Rincé et al. (1989) show tidally averaged concentrations at the surface at Saint-Nazaire up to 0.7 g/l during periods of high discharge, and concentrations in the range 0.05–0.1 g/l during periods of low river discharge. From remote sensing data, Gernez et al. (2015) also found concentrations at the surface in the range 0.05–0.1 g/l. Both studies show that the concentrations at the surface are significantly higher during spring tides than during neap tides. Recent measurements near Donges (km 9.5) show sediment concentrations in the range 0.1–1.0 g/l near the surface during periods of low river discharge (Jalón-Rojas et al., 2016), with almost one order of magnitude difference between concentrations during spring and neap tide.

Sediment from the watershed: during non-extreme discharge conditions, sediment supply from the watershed is relatively unimportant in the Loire. Concentrations at the upstream station of Montjean-sur-Loire have remained of a similar magnitude over the course of the 20th century with yearly averaged values of 20–40 mg/l, as reported by Berthois (1957) for the period 1953–1955, CSEEL (1984) for the period 1953–1981, and Sogreah (2010) for the period 2009–2010. During low flow conditions, concentrations are as small as 10 mg/l. Hence, in our model study, we did not account for sediment from the watershed.

Settling velocity: in-situ measurements of settling velocities using an Owen tube in 2008 are presented by Walther et al. (2012). Values are found to vary between 0.1 mm/s and over 2 mm/s roughly as a function of concentration. Settling velocities of around 1–2 mm/s are found for concentrations of about 1–2 g/l. For higher concentrations, these settling velocities decrease due to hindered settling. The default value used in the model was 2 mm/s, and the model accounts for the effects of hindered settling.

2.4. Calibration and Experiment Set-Up

We chose to select a default case with a low discharge of 250 m^3/s for presenting our first results in Section 3. The sensitivity to higher discharges is investigated in Section 4. Throughout this study, the cases of spring and neap tide are treated separately assuming dynamic equilibrium. This means that it is assumed that spring or neap conditions last long enough for the sediment concentrations to adapt and the dynamics of the transition between spring and neap tide is not considered. The default parameters used in the model are summarized in Table 2.

The hydrodynamic model was calibrated by setting the roughness such that the water level amplitudes and phases show a reasonable correspondence to the 2007–2014 observations in the year 2000 case for neap tide and low river discharge. Following Hamm and Walther (2009), we chose different values of the roughness downstream

Table 2
Default Parameter Values

		Spring	Neap	Source
Hydrodynamics				
A^0	D_2 water level amplitude at $x = 0$	2.30 m	1.28 m	SYVEL data
A^1	D_4 water level amplitude at $x = 0$	0.24 m	0.20 m	SYVEL data
ϕ^0	D_2 water level phase at $x = 0$	0	0	Definition
ϕ^1	D_4 water level phase at $x = 0$	−148°	−155°	SYVEL data
Q	River discharge	250 m^3/s		Low summer discharge (DREAL, 2019)
z_0^*	dimensionless roughness	0.01 ($x < 45$ km)		Calibration of neap D_2 tidal elevation
		0.05 ($x > 60$ km)		
Sediment				
c_{sea}	Sediment concentration at $x = 0$	0.2 g/l	0.5 g/l	Calibration and data (see Section 2.3)
K_h	Horizontal eddy diffusivity	100 m2/s		Estimated; results insensitive to this parameter
M	Erosion parameter	0.03 s/m		Calibration
$w_{s,0}$	Clear water settling velocity	2 mm/s		Walther et al. (2012)
c_{gel}	Gelling concentration	100 g/l		Estimated from Walther et al. (2012)

and upstream of Nantes (km 50). This corresponds to the observation that the bottom is predominantly muddy in the downstream reaches and sandy in the upstream reaches. Thus we calibrated the dimensionless roughness height (i.e., the roughness height scaled with the local depth, see Equations 6 and 7) to a value of $z_0^* = 0.01$ for $x < 45$ km and $z_0^* = 0.1$ for $x > 60$ km, with a smooth transition connecting the two values.

The sediment model was calibrated by setting the erosion parameter M (cf. Equation 5) and the tide-averaged depth-averaged seaward sediment concentration c_{sea}. We chose $M = 0.01$ s/m following Dijkstra, Schuttelaars, Schramkowski, and Brouwer (2019). The seaward sediment concentration was set to $c_{sea} = 0.2$ g/l for neap tide and $c_{sea} = 0.5$ g/l for spring tide.

As shown by Dijkstra et al. (2019b), one model setting may sometimes have two distinct solutions with low and high sediment concentrations. To make sure both solutions are retrieved in such cases, we used two ways of conducting experiments. In the first, we did our experiments starting from year 1900 conditions ($\alpha = 0$ in Equation 11), where we know from extensive testing that only one solution with fairly low concentrations exists. This solution was then used as initial condition for experiments with larger α. In the second, we started from year 2000 conditions, where, in the default case, only one solution with high concentrations exists. This solution was used as initial condition for experiments with smaller α. As the two initial conditions are in the attraction domains of different solutions, both solutions were retrieved.

3. Results

In this section we discuss the resulting water motion and sediment concentration in the default case, firstly focusing on the year 2000 and 1900 cases (Sections 3.1 and 3.2) and then investigating various values of α representing bed levels between 1900 and 2000 (Section 3.3). Finally, in Section 3.4 we present the mechanisms underlying the sediment dynamics.

3.1. Default Case—Summer in Year 2000

Figure 5 shows the water motion and sediment concentration in the default case for the year 2000 for neap and spring tide. Comparison of modeled water level amplitudes to observations for the summer season (panels a and b) shows that the overall subtidal, D_2 and D_4 water levels are captured, although the spring tide D_2 amplitude and D_4 amplitude are slightly overestimated. The fit for spring tide is nevertheless considered very satisfactory, given that the model was only calibrated for D_2 tides during neap tide (see Section 2.4).

10.1029/2023JC020273

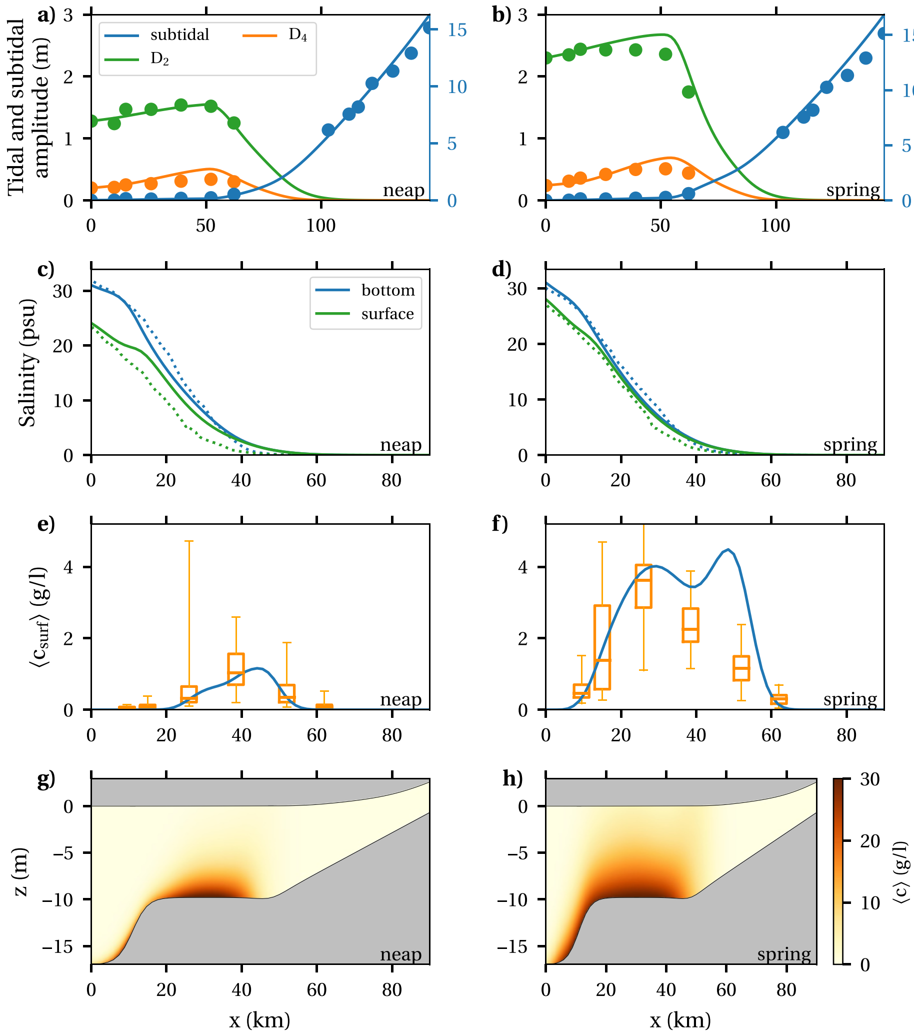

Figure 5. Model results for the default 2000 case for neap (left) and spring (right). Panels (a, b) show the surface amplitude compared against observations for the summer season (circles). The left vertical axis is for the D_2 and D_4 signals, while the right axis is for the subtidal set-up. Panels (c, d) show the salinity at the surface and bottom comparing our model results (solid lines) and thalweg concentrations from a 3D complex model (dotted lines). Panels (e, f) show the subtidal surface sediment concentration plotted against a boxplot with SYVEL observations near the surface for low discharges (Jalón-Rojas et al., 2016). Finally, panels (g, h) show along-channel sections of the modeled subtidal concentration.

In panels c and d, modeled salinity is compared to the thalweg salinity from a 3D complex model for similar discharge and tidal conditions. The overall salt intrusion length matches well and the stratification is captured over the first 15 km and underestimated >15 km. Importantly, the model correctly captures the larger salt stratification during neap tide compared to spring tide. Next, in panels e and f, modeled sediment concentrations are compared to the observed surface sediment concentration for low discharge (<200 m^3/s) (Jalón-Rojas et al., 2016). The model captures the order of magnitude of the surface concentration during spring and neap quite well. During neap, the maximum surface concentration is found a few km too far upstream. During spring, we find the correct ETM location and an additional secondary ETM that is not observed. Corresponding near-bed concentrations (panels e and f) are up to 30 g/l. Considering the simplicity of the model, the assumption of equilibrium and the focus on mechanisms rather than reproducing exact concentrations, we find this level of correspondence to observations satisfactory. Finally, panels g and h show the subtidal sediment concentration as a function of x and z, showing that near-bed sediment concentrations of up to 30 g/l are reached in the model.

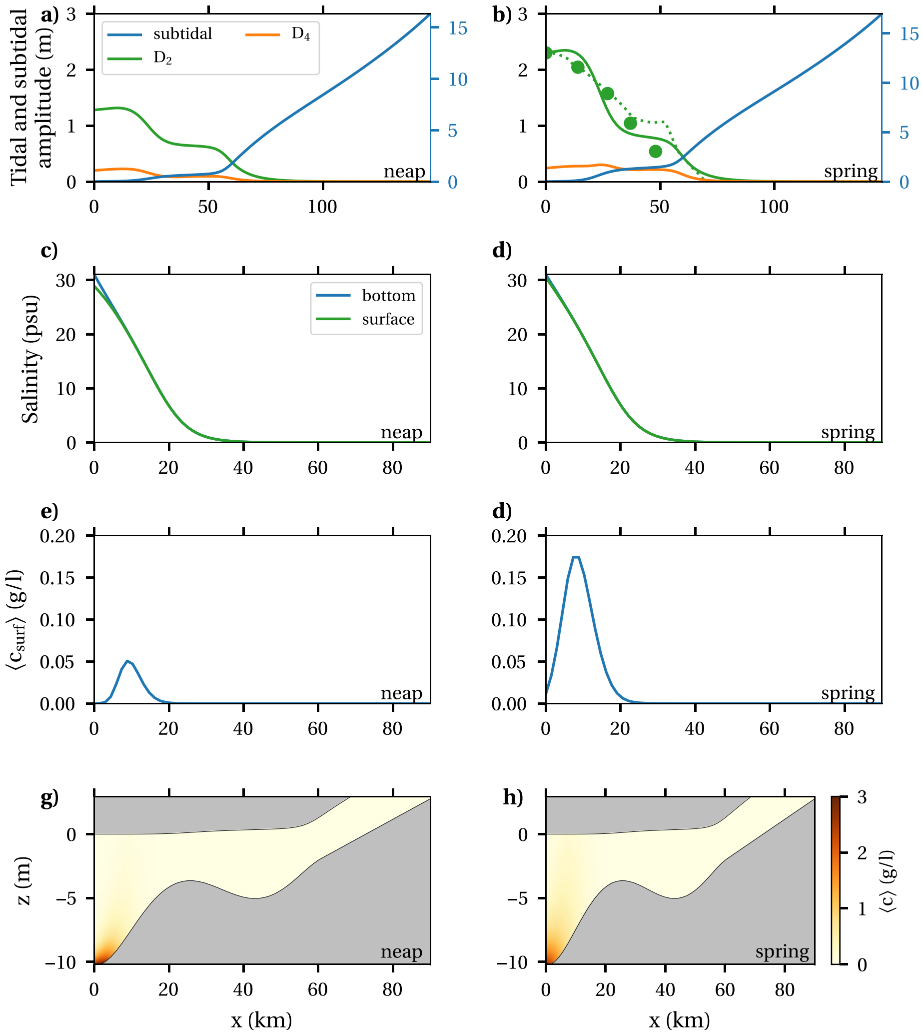

Figure 6. As Figure 5 for the year 1900 case. The spring D_2 tidal amplitude panel (b) is compared to 0.5 × the observed tidal range as reported by Paape (1994) (circles) and CSEEL (1984) (dotted).

3.2. Summer in Year 1900

To represent the year 1900, we only changed the bed level and kept all other parameters the same. The resulting surface elevation amplitude and sediment concentration are plotted in Figure 6. The tidal amplitude (panels a and b) is much more damped than in the year 2000 case. The modeled D_2 tidal amplitude is compared to the observed tidal range in 1900, divided by 2 to approximate the amplitude. The observed tidal range at the mouth is scaled to the same value as the model to compensate for slightly varying definitions of spring tide in the model and observations. The comparison shows a remarkably good fit, given that the model was not re-calibrated to year 1900 conditions. Salinity (panels c, d) shows almost no stratification in 1900. Sediment concentrations at the surface (panels e and f) are of the order of 0.1 g/l in the ETM, which is located close to the mouth (km 5–10). At the bottom (see panels g and h), sediment concentration reach up to 3 g/l. These concentrations occur at the mouth and are therefore controlled by the imposed value of c_{sea}.

3.3. Effect of Deepening Between 1900 and 2000

The effects of deepening on sediment concentrations were investigated by gradually varying the parameter α (Equation 11) from 0 (year 1900) to 1 (year 2000). Figures 7a and 7b shows the resulting tidally averaged near-bed (solid blue line) and near-surface (dashed orange line) sediment concentration in the ETM for neap and spring tide. To increase legibility, we categorized the concentrations as low (<1 g/l), intermediate (>1 g/l, <10 g/l), and

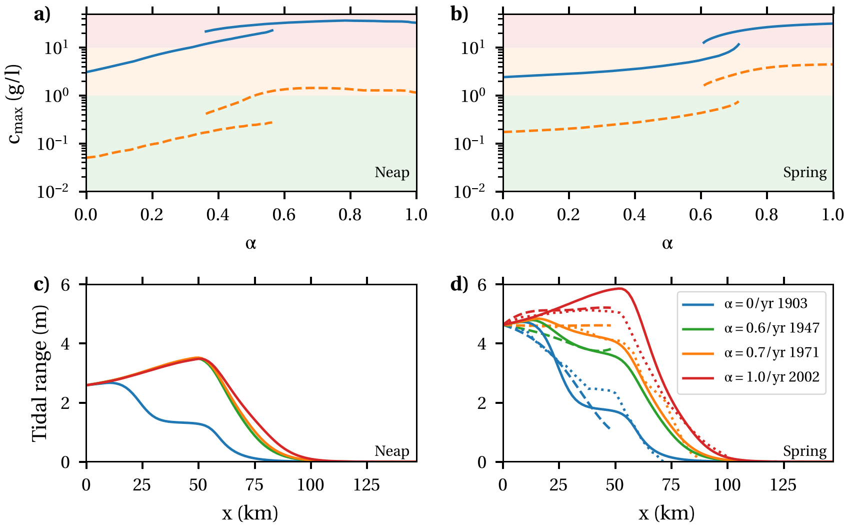

Figure 7. Results for the experiments with varying bed level parameter α (Equation 11) between 0 (year 1900) and 1 (year 2000) for neap (left) and spring (right). Panels a, b show the solutions for the subtidal concentration in the ETM near the bed (solid blue line) and surface (dashed orange line). The colors green, orange, red on the background are only indicative of low, intermediate and high concentrations. For certain values of α, two branches of solutions exists. Panels (c, d) show tidal range for a selection of values of α. Results for $\alpha = 0.6$ and $\alpha = 0.7$ in spring are on the lower solution branch. These are compared to observed tidal ranges for spring tide (dashed and dotted lines, see Figure 3c for references). Observations were scaled to the model results at $x = 0$ to compensate for varying definitions of spring tide.

high (>10 g/l). These definitions are simply practical and carry no further meaning. As α increases for $\alpha < 0.55$ (during neap, <0.75 during spring), the surface sediment concentration increases gradually for both neap and spring tide. The bottom concentration may even decrease. For α between 0.35 and 0.55 during neap tide, two solutions are observed. A similar result is found for spring tide for $0.6 < \alpha < 0.75$. Only the higher sediment concentration solution exists for larger α. Summarizing, lowering the bed level from 1900 conditions leads to gradually increasing sediment concentrations, followed by a catastrophic increase in the sediment concentration when α exceeds 0.55 (neap) or 0.75 (spring).

Figures 7c and 7d shows the tidal range resulting from the model simulations with $\alpha = 0, 0.6, 0.7$, and 1. For neap tide, the results for $\alpha \geq 0.6$ follow the higher sediment concentration solution branch. For spring tide, the results for $\alpha = 0.6$ and 0.7 are on the lower concentration branch. For both neap and spring tides, tidal range increases with increasing α on the low concentration branch, while it remains fairly constant on the high concentration branch. The model results are compared to observations for spring tide, plotted using dashed and dotted lines. The observed tidal ranges were scaled back to the same value as the model experiments at $x = 0$ to compensate for varying definitions of spring tide among the observations. We find that the tidal range in 1947 corresponds reasonably well to model results for $\alpha = 0.6$. The tidal range of 1971 corresponds best to model results for $\alpha = 0.7$.

3.4. Analysis of Mechanisms

Having established that the model shows a transition from low to high concentrations due to deepening, with sediment concentrations and water levels sufficiently resembling observations, we turn to the main goal of this study: identifying the underlying physical mechanisms.

Regime shift: first, we look at the sudden transition and possible existence of two solutions for the same model settings as we observed in Figure 7. The sudden transition is a mathematical bifurcation of the model, which is triggered by a strongly non-linear feedback mechanism. The mechanism is sketched in Figure 8 and extends work by Dijkstra, Schuttelaars, Schramkowski, and Brouwer (2019) and Lin et al. (2021) (see also Winterwerp and Wang (2013), Van Maren et al. (2015), and Van Maren et al. (2020)). Deepening leads to an increased capacity of the estuary to import sediment, which translates into higher equilibrium sediment concentrations. This in turn leads to stratification that reduces vertical mixing and bed friction, which further increases the sediment importing

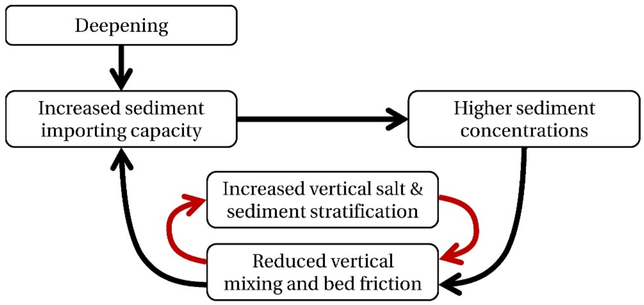

Figure 8. Feedback process enabling the regime shift. Adapted with some changes from Dijkstra, Schuttelaars, Schramkowski, and Brouwer (2019) and Lin et al. (2021).

capacity of the estuary. This mechanism is further reinforced because of a feedback between the reduction in vertical mixing and increasing salt and sediment stratification in the water column (red arrows). In the range of model settings where two solutions exist, the model apparently allows for one state in which this feedback remains weak, leading to low-intermediate concentrations, and one alternative state where this feedback is strong, leading to high concentrations.

Sediment transport capacity: next, the sediment transport capacity of the estuary, featuring prominently in Figure 8, is determined by many different physical contributions. Below, we investigate closer which contributions are important in the Loire and why they have changed so strongly over the century. Starting with the definition, the sediment transport capacity T is the tidally averaged amount of sediment that could be transported through a cross-section if there was plenty of sediment available on the bed. For intuition, one can imagine the transport capacity to measure the way in which any addition of sediment to an estuary in equilibrium would redistribute over the length of the estuary. This implies that an area where T changes sign from positive to negative corresponds to a convergence of sediment and hence a local maximum in the amount of sediment available. Thus, to study ETM, we look at zero crossings of T with $T_x < 0$.

Several individual contributions to the transport capacity are distinguished using our model. Below we describe the most important contributions in the Loire (see Dijkstra, Brouwer, et al. (2017) for a complete overview).

1. The *external D_4 tidal* contribution is due to tidal asymmetry caused by the D_2 and D_4 tides entering the estuary at the mouth and propagating into the estuary. The tidal asymmetry can imply higher maximum velocities during ebb or flood, which leads to a net sediment transport. Or it can imply a longer slack after HW or LW, leading more settling and hence lower concentrations at the start of the next ebb or flood, also leading to net transport. Note that the model also resolves the D_4 tide that is generated inside of the estuary by non-linear self-interaction of the D_2 tide. This contribution to the tidal asymmetry is considered separately in several other contributions, including the tidal return flow discussed below.
2. The *baroclinic* contribution is due to the covariance between the gravitational circulation and stratified sediment concentration profile. As concentrations are larger near the bed than near the surface and gravitational circulation is directed upstream near the bed, this usually results in an upstream transport. Note that our model exclusively resolves gravitational circulation and not other density-driven contributions to the exchange flow, such as the ESCO circulation (Dijkstra, Schuttelaars, & Burchard, 2017).
3. The *spatial settling lag* contribution (e.g., De Swart & Zimmerman, 2009) tends to transport sediment toward along-channel minima in the tidal velocity amplitude or sediment concentration.
4. The *tidal return flow* contribution is the transport capacity due to Stokes drift and the corresponding return flow. The Stokes drift causes sediment import, while the return flow usually causes a somewhat larger export. Additionally, the return flow velocity has a D_4 contribution generated by self-interaction of the D_2 tide, which may cause import or export of sediment, depending on the phase-lag with the D_2 tide.
5. The *river* contribution reflects the effects of river discharge in both flow and re-suspension of sediment.

Figure 9 shows these transport capacity contributions T for the neap tide case for the year 1900 (panel a) and 2000 (panel b). Results for spring tide are qualitatively the same and hence not shown. In 1900, the transport capacity is dominated by export (negative transport capacity) by the river, compensated only by a small import due to the external tidal asymmetry, baroclinic transport, and sediment advection. The total transport capacity (black line) however remains negative, indicating that no ETM will form. In 2000, the same transport contributions are dominant, but the importing contributions are much stronger. Import is dominated by the external tidal asymmetry in the entire estuary, the baroclinic transport in the first 20 km and sediment advection for $x > 20$ km.

Figure 9c shows the same transport contributions plotted in one panel and on a log-scale to highlight the differences between 1900 (dashed lines) and 2000 (solid lines). In order to explain the changes in transport capacity between 1900 and 2000 we will also compare the depth-averaged velocities (panel d) and eddy viscosity/diffusivity (panel e) between the two cases. The changes are discussed here for each mechanism.

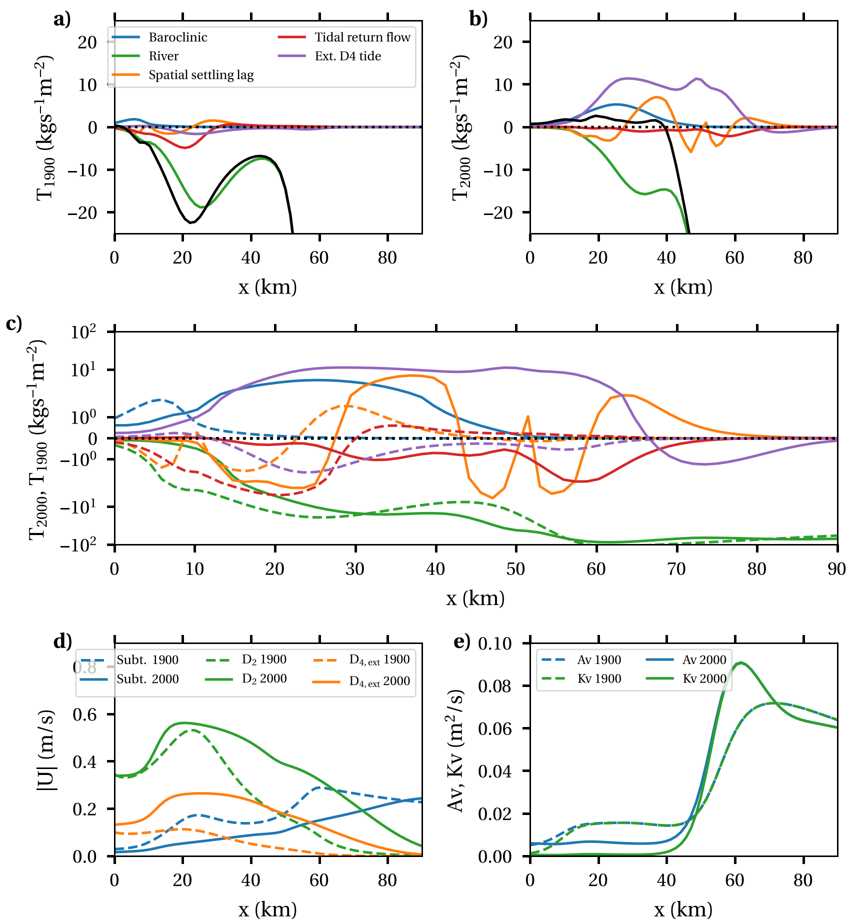

Figure 9. Panels (a–c) show the 5 most dominant contributions to the transport capacity and the sum of all contributions (black line). Panels a, b show the results for the default case for neap in 1900 and 2000. Panel c shows the same results for 1900 (dashed) and 2000 (solid) in one plot and on a logarithmic scale. Panel d shows the depth-averaged subtidal velocity and tidal D_2 and D_4 velocity amplitudes ($|\overline{u}|$) for the default neap case in 1900 and 2000. Panel e shows the eddy viscosity (A_ν) and eddy diffusivity (K_ν) for the default neap case in 1900 and 2000.

- The exporting capacity by the river discharge changed least significantly, increasing by no more than a factor 2 locally. The reason for is twofold: firstly, the river discharge has remained the same, so that sediment is transported over a larger cross-section in 2000 but at lower river-induced velocity (Figure 9d). Secondly, resuspension has not changed much; for $x < 50$ km resuspension is dominated by the D_2 tidal velocity, which increased only up to a factor 2 (Figure 9d). For $x > 50$ km subtidal flow and D_2 are both important for resuspension and the decrease in subtidal flow approximately compensates the increase in D_2 flow.
- The baroclinic transport capacity changed very significantly, increasing by up to factor 10 from 1900 to 2000 and shifting upstream. This is related to the increased depth and a decrease in turbulent mixing due to the salt- and sediment-induced damping of turbulence (Figure 9e). The eddy viscosity in the area between 15 and 50 km has decreased by a factor 2.5, while the eddy diffusivity has decreased by a factor 20. The relative importance of salt and sediment induced damping on the reduction is further discussed below. The large increase in baroclinic transport capacity can easily be understood using classical theory: it is the product of the gravitational circulation and subtidal vertical sediment concentration profile for which analytical solutions are available that show strong dependence on depth and eddy viscosity/diffusivity (see Festa & Hansen, 1978; Geyer, 1993).
- The biggest change occurred in the external tidal transport capacity. While this was a small and primarily exporting contribution in 1900, it is the dominant importing contribution in 2000. There are various causes for this. Firstly, we look at the depth-averaged velocity amplitude ($|U|$), plotted in Figure 9d. The D_2 velocity amplitude (green lines in Figure 9d) changed little in the first 20 km and up to a factor 2 at km 40. The D_4

10.1029/2023JC020273

velocity amplitude related only to the tide forced at the estuary mouth (orange lines) on the other hand changed more than a factor 2 in the first 20 km and up to a factor 5 at km 40. Clearly, the amplification of the D_4 tide is most dominant. Secondly, this velocity transports sediment over a larger depth. Finally, the phase difference between the D_2 and D_4 tide (not shown) became favorable toward sediment import. All these effects are partly caused by deepening and partly by the sediment-induced reduction of turbulence.

- The sediment advection also changed strongly as it scales with along-channel gradients in the sediment carrying capacity. These gradients have increased, mainly because the eddy viscosity and eddy diffusivity vary strongly between the ETM and the rest of the estuary, leading to large differences in carrying capacity in each of these regions.
- Finally, the transport related to tidal return flow only changed mildly and this mechanism is not dominant. This transport is exporting in most of the estuary in both years. The observed increase in magnitude mainly reflects the increase in tidal water level amplitude for $x < 20$ km, as the D_2 velocity did not change much there.

The significant decrease in eddy viscosity and eddy diffusivity as shown in Figure 9e is related to the changes in depth, D_2 tidal velocity and stratification. Between 1900 and 2000, both the depth and tidal velocity amplitude (Figure 9d) increased, which would correspond to an increase in eddy viscosity and eddy diffusivity. Hence, the decrease in these turbulence parameters is entirely due to stratification. An additional comparison between the year 2000 case with and without stratification-induced damping of turbulence (i.e., setting $\overline{Ri} = 0$) is presented in the SI shows that high sediment concentrations are not attained if stratification is turned off, hence further confirming that stratification is important to take into account.

Summarizing, we saw that the dominant contributions to the sediment importing capacity of the estuary are the sediment transport related to the propagation of the external D_4 tide and the baroclinic flow, which are both highly sensitive to increasing depth and the reduced turbulence due to the increasing sediment concentrations. Results indeed show that the turbulence, measured by the eddy viscosity and eddy diffusivity has decreased very significantly up to km 50.

Relative importance of sediment- and salt-induced turbulence damping: both sediment and salt stratification contribute significantly to the reduction of turbulence. To assess the importance of the two processes, we look at the relative contribution they make to the depth-averaged Richardson number (see Equation 8). In the year 2000 case for neap conditions, the relative contribution of salt stratification to the depth-averaged subtidal Richardson number is 60% at the mouth, decreasing to 20% at km 20 and further to 0 at km 50. Hence, the contribution of salt stratification is especially significant close to the mouth, while sediment stratification is dominant in the ETM. It should be noted here that salt stratification is our model is underestimated compared to the real stratification in the thalweg upstream from km 15, so the relative contribution of salinity should possibly be larger, yet still not bigger than the contribution by sediment stratification.

While salt stratification is important, salt stratification without sediment stratification is not sufficient to trigger the regime shift with two solution branches. The reason for this is the negative (i.e., self-stabilizing) feedback in salinity dynamics: salt stratification leads to reduced mixing, which leads to increased salt intrusion. The reduced along-channel salinity gradient in turn moderates the stratification, so the process is not self-reinforcing.

4. Sensitivity Analysis

We have established the development of hyperturbid conditions in the Loire in the model for summer conditions with default parameters. In this section we show the robustness of the results to higher discharges and other parameter choices. Firstly, in Section 4.1, we focus on the year 2000 and the effect of imposing a higher river discharge representing other seasons. Next, in Section 4.2, we investigate the effect of choosing other values for the most important uncertain and variable parameters on the regime shift between 1900 and 2000.

4.1. Effect of Discharge in 2000

We investigated the effect of the river discharge on the occurrence of hyperturbidity in the year 2000. The discharge is varied between 100 and 1,500 m^3/s, where we recall that the year-average discharge is 910 m^3/s and the winter-average is 1,300 m^3/s. As in the previous experiments, we computed dynamic equilibrium, that is, assuming a constant discharge for a long time. We also varied the seaward sediment concentration, inspired by for example, Rincé et al. (1989), who describe that seaward concentrations increase with increasing discharge as

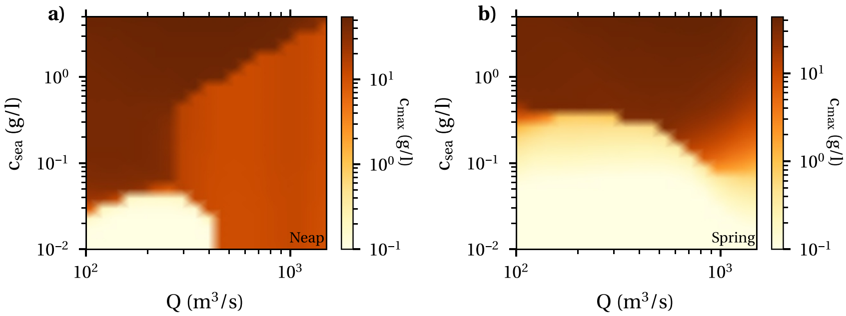

Figure 10. Subtidal near-bed concentration in the ETM as a function of river discharge and seaward sediment concentration for neap (left) and spring (right) for the year 2000 case.

sediments are flushed to the estuary mouth. As described in Section 2.3, observed sediment concentrations at $x = 0$ at the surface vary over one order of magnitude from less than 0.1 g/l to over 1 g/l. Here we choose a range for the depth-averaged subtidal concentration c_{sea} from 10^{-2}-5 g/l, thereby covering all possible model behavior and covering the observed range.

Figure 10 shows the results of the sensitivity study for neap (panel a) and spring (panel b), combining results of over 1,100 model experiments. The color indicates the tidally averaged near-bed sediment concentration in the ETM as a function of discharge and depth-averaged seaward sediment concentration. In the area with dark orange colors, high sediment concentrations (>10 g/l) occur. Provided sufficiently high seaward concentrations are imposed ($c_{sea} > 0.05$ g/l for neap and >0.4 for spring), such high concentrations were found for all discharges up to 1,500 m^3/s. For discharges roughly larger than 300 m^3/s, the ETM moves downstream from its summer location between km 30–50 to around km 10 and moving slightly further downstream with increasing discharge while remaining inside the estuary; that is, maximum sediment concentrations in the estuary are larger than at the boundary. These results qualitatively match observations, which also show the ETM moving downstream but not really leaving the estuary (CSEEL, 1984; Jalón-Rojas et al., 2016).

As the ETM moves to the zone near km 10 for larger discharges, gravitational circulation becomes the dominant importing mechanism and the tidal transport is negligible. Clearly in the model, the transport by gravitational circulation is thus the reason the ETM is not flushed from the estuary at higher discharges and an important process for maintaining higher sediment concentrations throughout the seasons.

4.2. Combined Effect of Various Uncertain Parameters and Deepening

In our default case in Section 3.3 we found that sediment concentrations were low in 1900 and high in 2000 with the transition possible for α between 0.35 and 0.75 (neap and spring combined). However, parameters such as the river discharge Q and seaward sediment concentration c_{sea} are not constant in time and the settling velocity $w_{s,0}$ is uncertain. In this section we therefore investigate whether the regime shift occurs for a wider range of parameter settings and if it does, at what value of α. For brevity, in this section we focus on creating a broader image of the regime shift under these parameter variations, without explaining the underlying parameter sensitivity in detail. To this end, we investigated the regime shift as a function of the bed level parameter α and the three parameters mentioned above: Q in the range 100–1,500 m^3/s, c_{sea} in the range 0.05–5 g/l and $w_{s,0}$ in the range 0.5–3 mm/s. We concentrated only on the neap tidal case and carried out our simulations by reducing α from 1 to 0, so that we retrieved the solution with highest sediment concentration in case multiple solutions exist. In total, this study consists of 13,200 model experiments.

Figure 11 shows the results in the form of a two-dimensional histogram. The histogram in Figure 11a shows the fraction of model experiments (indicated by the shade of red) for a certain α (horizontal axis) resulting in a certain tidally averaged near-bed concentration in the ETM (vertical axis). The gray lines are drawn to increase legibility and again indicate the low, intermediate concentrations, and high concentrations as before. We observe that many of the model experiments are result in maximum near-bed concentrations around 1 g/l. As α increases, an increasing number of simulations attains maximum concentrations of the order of 30 g/l, showing that the

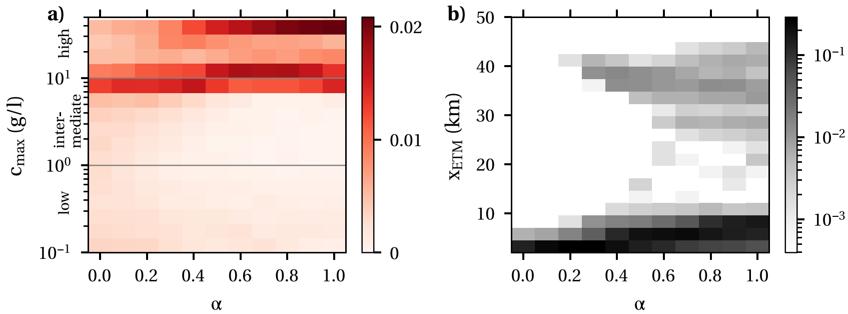

Figure 11. Two-dimensional histogram of the sensitivity study for Q, c_{sea}, and $w_{s,0}$ plotted against the bed level parameter α. Colors indicate the fraction of experiments in its respective two-dimensional bin. Panel a plots the histogram for the subtidal near bed concentration in the ETM. Panel b plots the histogram for the ETM location.

hyperturbid state becomes ever more robust as depth increases. At the same time, the number of simulations with low concentrations decreases with increasing depth.

Figure 11b shows a similar histogram with the ETM location on the vertical axis. For the 1900 case ($\alpha = 0$), the ETM is exclusively found near the mouth. For increasing α beyond roughly value of 0.3 the ETM shifts upstream and either one of two possible ETM regions is realized: between km 0 and 10 (LOC1) and one varying between km 25 and 40 (LOC2). Further analysis shows that only high concentrations occur in LOC2, while LOC1 may feature low or high concentrations, depending on conditions. The main conclusion for our study is that any high concentration that would occur in 1900 was focussed near the mouth, while for $\alpha > 0.2$ this could occur deeper into the estuary.

Overall, we draw several conclusions. Firstly, the mechanism causing hyperturbid conditions in the interior estuary was absent in the 1900 case. Secondly, increasing depth increasingly allows for the occurrence of high sediment concentrations and a shift of the ETM to the interior estuary. And finally, the sudden jump to high sediment concentrations observed in the default case is more widely present. Within our range of experiments this may start to occur for $\alpha > 0.3$.

5. Discussion

5.1. Interpretation of the Regime Shift and Limitations

The simplified nature of the used model poses several limitations. In this section we discuss these limitations and how they affect the interpretation of the results. Specifically, we focus on the physical mechanisms and the time at which the transition occurred.

Firstly, several processes are not explicitly included in this study. Temporally varying eddy viscosity/eddy diffusivity is not explicitly accounted for, so the model does not account for mud-induced periodic stratification (Becker et al., 2018) and the resulting ESCO circulation (Dijkstra, Schuttelaars, & Burchard, 2017). Furthermore, all lateral processes and interactions with tidal flats are not explicitly resolved. We have also not accounted explicitly for sediment flocculation, critical shear stress, and consolidation. While explicitly accounting for these additional processes will affect the sediment dynamics, this study showed that these mechanisms are not essentially needed for reproducing some of the main characteristic of the regime shift in the Loire.

Secondly, one should be careful inferring the time at which the regime shift occurred from these results. The model results show that the regime shift may have occurred for bed level parameters ranging from anywhere between $\alpha = 0.3$ and $\alpha = 1$, leaving a time window of several decades during which the regime shift could have occurred. The model simply states that a regime shift is possible during this window, given that certain conditions (i.e., certain discharge and tidal conditions) pertain for long enough to reach dynamic equilibrium. In reality, the estuary is constantly adapting to a changing dynamic equilibrium. Therefore, an actual observation of the regime shift is not a sudden transition, but rather occurs gradually over time. Comparing tidal records and model solutions, the transition period in the Ems river was estimated to take about 6 years starting roughly around 1989 (Dijkstra et al., 2019b). A similar estimate for the Loire is not yet available.

Given that the actual transition to high concentrations in the Loire was a gradual process means that it will be hard to determine whether the bifurcation (or regime shift) found using our model is representative for reality. Alternatively, the real estuary could be strongly sensitive to deepening but possibly without having two equilibrium states or sudden transitions. Either way, the described essential processes described in Figure 8 and Section 3.4 are an explanation for the extreme increase of the sediment concentration.

5.2. Comparing to the Ems and Implications for Other Estuaries

Many of the World's estuaries are deepened and some may run the risk of experiencing a similar transition to hyperturbid conditions as in the Loire. Our current knowledge is insufficient to state the general characteristics of estuaries at risk. Therefore it is useful to emphasize the characteristics found to be essential in the Loire and compare this to the Ems.

In both the Loire and Ems, deepening set off a positive feedback between increasing sediment concentration, salt- and sediment-induced damping of turbulence, and sediment import (cf. Figure 8). Two candidates for sediment import processes featuring in this feedback loop have been identified. Firstly, the tidal asymmetry related to the D_2 and D_4 tide already present at the estuary mouth and propagating into the estuary play a crucial role in both the Loire and Ems rivers (Dijkstra, Schuttelaars, Schramkowski, & Brouwer, 2019). The relative phase difference between the D_2 and D_4 tide is such that the tidal asymmetry causes sediment import in both rivers. This sediment import contribution amplifies greatly under the aforementioned feedback process. In the Ems, this strong amplification of sediment import was attributed to resonance of the D_4 tide. While resonance is meaningful in the Ems, where tides reflect against a weir at the landward boundary, the Loire has no strict upstream boundary, so tidal resonance is not meaningful. Nevertheless, tidal amplification behaves similarly in both estuaries. Further research is needed to determine the specific geometric and bathymetric characteristics that are responsible for this amplification of the D_2 and especially the D_4 tide.

Secondly, sediment import related to gravitational circulation was found to be important in the feedback loop in the Loire and the dominant process for discharges larger than the typical summer conditions. This transport was found to be less significant in the Ems. This new insight implies that we should consider the possibility of a transition to hyperturbid conditions also in estuaries where sediment transport is dominantly controlled by gravitational circulation. The strong dependence of sediment transport by gravitational circulation to deepening and reduction of vertical mixing can easily be understood from the theory of Festa and Hansen (1978) and Geyer (1993). Furthermore, Van Maren et al. (2020) already suggested that this transport contribution could potentially be important in the mentioned feedback loop.

6. Conclusions

In this study we investigated the transition to hyperturbid conditions in the Loire estuary, with our main results covering a review of observations, a qualitative model reconstruction of the regime shift and an analysis of the physical mechanisms governing the regime shift. Firstly, while the Loire was discussed in literature as system where a regime shift occurred, a review of observations showing this was missing. Therefore, we provided an overview of historical sediment observations. These show sediment concentrations have indeed increased by an order of magnitude at the surface, mainly after 1990. Thick layers of fluid mud near the bed probably already occurred much earlier, possibly becoming more extensive already in the 1970s. Additionally, the ETM moved upstream over the decades.

Secondly, we performed an idealized width-averaged model study. Calibrating the model to a case representing the year 2000 we find satisfactory comparison between model results and observed tidal elevation and sediment concentrations. Varying the bed level between conditions in 1900 and 2000, keeping all other model parameters the same, the models shows a bifurcation or regime shift, where the equilibrium sediment concentration suddenly increases past a certain bed level threshold. Also, for certain bed levels, the model suggests the existence of multiple stable states. The value of the bed level threshold depends on the forcing of the estuary (tide, river discharge) and model parameters and hence we cannot uniquely identify one threshold value. However, we do find that high sediment concentrations would have been extremely unlikely to occur in the Loire in 1900, while hyperturbid conditions are found in the year 2000 for most conditions.

Thirdly, we analyzed the dominant sediment transport processes causing the regime shift. This first is the transport caused by the tidal asymmetry, where especially the tidal asymmetry caused by the D_4 tide entering the estuary from the mouth is important. While in a previous study on the Ems estuary this could be attributed to tidal resonance, there is no clear tidal reflector (e.g., weir or dam) in the Loire. A new finding is therefore that the amplification of the tidal asymmetry apparently is not dependent on resonance. The second mechanism is the transport due to gravitational circulation. This mechanism is always important in the Loire and dominant when the ETM is in the salt water zone, that is, when the discharge is larger than typical summer conditions. While this transport mechanism is well known, this is the first time this mechanism is explicitly shown to play an important role in a transition to hyperturbid conditions. With both identified transport processes, the feedback between increased import, increased sediment concentration and reduced turbulence is essential for establishing the regime shift. Additional to the transport processes, we identified that salt stratification played an important role in the reduction of turbulence. While sediment stratification remains essential to generate the observed regime shift and multiple stable states, salt stratification further reinforces the feedback process.

Data Availability Statement

The iFlow model used for this study, together with tutorial and input files are available under version 3.2 on GitHub/Zenodo (iFlow modelling framework (Version 3.2), 2024).

Acknowledgments

This work is partly based on the MSc thesis of Roel de Goede (http://resolver.tudelft.nl/uuid:1705a083-17c0-461c-b17c-231ec28f4860), which was financially supported by the project "KPP Schelde-estuarium" assigned to Deltares by the Dutch Directorate-General for Public Works and Water Management (Dutch: "Rijkswaterstaat").

References

Allen, G., Salomon, J., Bassoullet, P., Penhoat, Y. D., & de Grandpré, C. (1980). Effects of tides on mixing and suspended sediment transport in macrotidal estuaries. *Sedimentary Geology*, *26*(1–3), 69–90. https://doi.org/10.1016/0037-0738(80)90006-8

Becker, M., Maushake, C., & Winter, C. (2018). Observations of mud-induced periodic stratification in a hyperturbid estuary. *Geophysical Research Letters*, *45*(11), 5461–5469. https://doi.org/10.1029/2018gl077966

Berthois, L. (1954). La sédimentation en Loire en grande marée de vive eau. *Comptes Rendus hebdomadaires des séances de l'Académie des Sciences*, *240*, 106–108.

Berthois, L. (1955). Sédimentation dans l'estuaire de la Loire en période hivernale. *Comptes Rendus hebdomadaires des séances de l'Académie des Sciences*, *236*, 1984.

Berthois, L. (1957). Comportement du "bouchon vaseux" dans l'estuaire de la Loire. In *Les énergies de la mer. compte rendu desquatrièmes journées de l'hydraulique, paris* (Vol. 13, p. 14)

Berthois, L., & Barbier, M. (1953). La sedimentation en Loire maritime en période d'étiage. *Comptes Rendus hebdomadaires des séances de l'Académie des Sciences*, *236*, 1984–1986.

Briere, C., Giardino, A., & Winterwerp, J. (2011). *Analyse de la morphologie du chenal de Nantes et étude de sa restauration: Phase 1: evolutions passées et fonctionnement actuel*. (Tech. Rep. No. 1201695). Deltares.

Brouwer, R. L., Schramkowski, G. P., Dijkstra, Y. M., & Schuttelaars, H. M. (2018). Time evolution of estuarine turbidity maxima in well-mixed, tidally dominated estuaries: The role of availability- and erosion-limited conditions. *Journal of Physical Oceanography*, *48*(8), 1629–1650. https://doi.org/10.1175/jpo-d-17-0183.1

Burchard, H., & Baumert, H. (1998). The formation of estuarine turbidity maxima due to density effects in the salt wedge. a hydrodynamic process study. *Journal of Physical Oceanography*, *28*(2), 309–321. https://doi.org/10.1175/1520-0485(1998)028⟨0309:tfoetm⟩2.0.co;2

Burchard, H., Schuttelaars, H. M., & Ralston, D. K. (2018). Sediment trapping in estuaries. *Annual Review of Marine Science*, *10*(1), 371–395. https://doi.org/10.1146/annurev-marine-010816-060535

Chernetsky, A. S., Schuttelaars, H. M., & Talke, S. A. (2010). The effect of tidal asymmetry and temporal settling lag on sediment trapping in tidal estuaries. *Ocean Dynamics*, *60*(5), 1219–1241. https://doi.org/10.1007/s10236-010-0329-8

CSEEL. (1984). *Rapport final du comité scientifique pour l'environnement de l'estuaire de la Loire*. (Tech. Rep.). Centre National pour l'Exploitation des Océans, Brest, France. (Rapports Scientifiques et Techniques, no 55).

De Jonge, V. N., Schuttelaars, H. M., Van Beusekom, J. E. E., Talke, S. A., & De Swart, H. E. (2014). The influence of channel deepening on estuarine turbidity levels and dynamics, as exemplified by the Ems estuary. *Estuarine, Coastal and Shelf Science*, *139*, 46–59. https://doi.org/10.1016/j.ecss.2013.12.030

De Swart, H., & Zimmerman, J. (2009). Morphodynamics of tidal inlet systems. *Annual Review of Fluid Mechanics*, *41*(1), 203–229. https://doi.org/10.1146/annurev.fluid.010908.165159

Dijkstra, Y. M., Brouwer, R. L., Schuttelaars, H. M., & Schramkowski, G. P. (2017a). The iFlow modelling framework v2.4. A modular idealized process-based model for flow and transport in estuaries. *Geoscientific Model Development*, *10*(7), 2691–2713. https://doi.org/10.5194/gmd-10-2691-2017

Dijkstra, Y. M., Schuttelaars, H. M., & Burchard, H. (2017b). Generation of exchange flows in estuaries by tidal and gravitational eddy viscosity - Shear covariance (ESCO). *Journal of Geophysical Research: Oceans*, *122*(5), 4217–4237. https://doi.org/10.1002/2016jc012379

Dijkstra, Y. M., Schuttelaars, H. M., & Schramkowski, G. P. (2019a). Can the Scheldt River estuary become hyperturbid? A model analysis of suspended sediment concentrations and transport in response to channel deepening. *Ocean Dynamics*, *69*(7), 809–827. https://doi.org/10.1007/s10236-019-01277-z

Dijkstra, Y. M., Schuttelaars, H. M., & Schramkowski, G. P. (2019b). A regime shift from low to high sediment concentrations in a tide-dominated estuary. *Geophysical Research Letters*, *46*(8), 4338–4345. https://doi.org/10.1029/2019gl082302

Dijkstra, Y. M., Schuttelaars, H. M., Schramkowski, G. P., & Brouwer, R. L. (2019c). Modeling the transition to high sediment concentrations as a response to channel deepening in the Ems River Estuary. *Journal of Geophysical Research: Oceans*, *124*(3), 1–17. https://doi.org/10.1029/2018JC014367

Dijkstra, Y. M., Schuttelaars, H. M., & Winterwerp, J. C. (2018). The hyperturbid state of the water column in estuaries and rivers: The importance of hindered settling. *Ocean Dynamics*, *68*(3), 377–389. https://doi.org/10.1007/s10236-018-1132-1

DREAL. (2019). La Loire à Montjean-sur-Loire - Synthese: données hydrologiques de synthèse (1863–2019). Retrieved from http://www.hydro.eaufrance.fr/

Ferret, Y. (2016). *Reconstruction de la série marégraphiquede Saint-Nazaire*. (Tech. Rep.). SHOM.

Festa, J. F., & Hansen, D. V. (1978). Turbidity maxima in partially mixed estuaries: A two-dimensional numerical model. *Estuarine and Coastal Marine Science*, *7*(4), 347–359. https://doi.org/10.1016/0302-3524(78)90087-7

Gallenne, B. (1974a). *Les accumulations turbides de l'estuaire de la loire. etude de la "crème de vase" (Unpublished doctoral dissertation)*. University of Nantes.

Gallenne, B. (1974b). Study of fine material in suspension in the estuary of the Loire and its dynamic grading. *Estuarine and Coastal Marine Science*, *2*(3), 261–272. https://doi.org/10.1016/0302-3524(74)90016-4

Gasowski, Z. (1994). L'enfoncement du lit de la Loire/the entrenchment of the Loire's river bed. *Revue de Geographie de Lyon*, *69*(1), 41–45. https://doi.org/10.3406/geoca.1994.4236

Ge, J., Zhou, Z., Yang, W., Ding, P., Chen, C., Wang, Z. B., & Gu, J. (2018). Formation of concentrated benthic suspension in a time-dependent salt wedge estuary. *Journal of Geophysical Research: Oceans*, *123*(11), 8581–8607. https://doi.org/10.1029/2018jc013876

Gernez, P., Lafon, V., Lerouxel, A., Curti, C., Lubac, B., Cerisier, S., & Barillé, L. (2015). Toward sentinel-2 high resolution remote sensing of suspended particulate matter in very turbid waters: Spot4 (take5) experiment in the Loire and Gironde estuaries. *Remote Sensing*, *7*(8), 9507–9528. https://doi.org/10.3390/rs70809507

Geyer, W. R. (1993). The importance of suppression of turbulence by stratification on the estuarine turbidity maximum. *Estuaries*, *16*(1), 113. https://doi.org/10.2307/1352769

GIP. (2002). Les amplitudes de l'onde de marée. Retrieved from https://www.loire-estuaire.org/upload/espace/1/pj/43670_2824_CMB_206106_L1A1.pdf

GIP. (2004). Les niveaux d'eau de la Maine à la Mer. Retrieved from http://www.loire-estuaire.org/upload/iedit/1/pj/43662_1922_panneau_NiveauxEaux.pdf

GIP. (2011). Equilibre du lit de la Loire estuarienne - Lancement d'un programma d'actions 2012-2020. Retrieved from http://www.loire-estuaire.org/upload/espace/1/pj/44124_2657_dossier_lettre14.pdf

GIP. (2014). *Atlas morpho-bathymétrique la Loire de Nantes à Saint-Nazaire*. (Tech. Rep.). GIP Loire estuaire. Retrieved from http://www.loire-estuaire.org/accueil/nos_ressources/publications.InFrench

Grasso, F., & Caillaud, M. (2023). A ten-year numerical hindcast of hydrodynamics and sediment dynamics in the Loire Estuary. *Scientific Data*, *10*(394), 394. https://doi.org/10.1038/s41597-023-02294-w

Guilcher, A. (1988). Léopold berthois (1900–1986). une carrière exemplaire au service de la mer, ses côtes, ses fonds et ses sédiments. *Norois*, *138*(1), 191–200. https://doi.org/10.3406/noroi.1988.4403

Hamm, L., & Walther, R. (2009). Morphodynamic coupling of bottom roughness and fluid mud for modelling tidal propagation in the Loire estuary (France). In *Coastal engineering 2008: (in 5 volumes)* (pp. 2832–2841). World Scientific.

iFlow modelling framework (Version 3.2). (2024). iFlow modelling framework (Version 3.2) [Software]. *GitHub/Zenodo*. https://doi.org/10.5281/zenodo.809944

Jalón-Rojas, I., Schmidt, S., Sottolichio, A., & Bertier, C. (2016). Tracking the turbidity maximum zone in the Loire Estuary (France) based on a long-term, high-resolution and high-frequency monitoring network. *Continental Shelf Research*, *117*, 1–11. https://doi.org/10.1016/j.csr.2016.01.017

Le Hir, P. (1994). Fluid and sediment integrated modelling application of fluid mud flows in estuaries. In *Cohesive sediments, proceedings of intercoh 1994* (pp. 417–428).

Lin, J., van Prooijen, B. C., Guo, L., Zhu, C., He, Q., & Wang, Z. B. (2021). Regime shifts in the Changjiang (Yangtze River) Estuary: The role of concentrated benthic suspensions. *Marine Geology*, *433*, 106403. https://doi.org/10.1016/j.margeo.2020.106403

MacCready, P. (2004). Toward a unified theory of tidally-averaged estuarine salinity structure. *Estuaries*, *27*(4), 561–570. https://doi.org/10.1007/BF02907644

Manning, A. J., Langston, W. J., & Jonas, P. J. C. (2010). A review of sediment dynamics in the Severn Estuary: Influence of flocculation. *Marine Pollution Bulletin*, *61*(1–3), 37–51. https://doi.org/10.1016/j.marpolbul.2009.12.012

Migniot, C. (1993). Bilan de l'hydrologie et de l'hydrosédimentaire de l'estuaire de la Loire au cours des deux dernières décénnies. *Association pour la Protection de l'Environnement de l'Estuaire de la Loire, Port Autonome de Nantes-St Nazaire, Nantes*.

Munk, W. H., & Anderson, E. R. (1948). Notes on a theory of the thermocline. *Journal of Marine Research*, *7*, 276–295.

Normant, C. L. (2000). Three-dimensional modelling of cohesive sediment transport in the Loire estuary. *Hydrological Processes*, *14*(13), 2231–2243. https://doi.org/10.1002/1099-1085(200009)14:13<2231::aid-hyp25>3.3.co;2-r

Paape. (1994). *Etude hydrologique de l'estuaire de la Loire*. (Tech. Rep. No. T1109/Z581). WL – Delft Hydraulics.

Richardson, J. F., & Zaki, W. N. (1954). The sedimentation of a suspension of uniform spheres under conditions of viscous flow. *Chemical Engineering Science*, *8*(2), 65–78. https://doi.org/10.1016/0009-2509(54)85015-9

Rincé, Y., Martin-Jézéquel, V., & Ravail, B. (1989). Ecological observations on plankton of the Loire estuary (France). *Cahiers de Biologie Marine*, *30*(2), 201–216.

Rosales-Sierra, V., & Levacher, D. (2004). Simulation numérique de l'estuaire de la Loire. In *Viiièmes journées nationales génie civil – génie côtier, compiègne* (pp. 7–9).

Saliot, A., Lorre, A., Marty, J.-C., Scribe, P., Tronczynski, J., Meybeck, M., et al. (1984). Biogéochimie de la matière organique en milieu estuarien: stratégies d'échantillonnage et de recherche élaborées en Loire (France). *Oceanologica Acta*, *7*(2), 191–207.

Schmidt, S., Diallo, I. I., Derriennic, H., Fallou, H., & Lepage, M. (2019). Exploring the susceptibility of turbid estuaries to hypoxia as a prerequisite to designing a pertinent monitoring strategy of dissolved oxygen. *Frontiers in Marine Science*, *6*. https://doi.org/10.3389/fmars.2019.00352

Scully, M. E., & Friedrichs, C. T. (2007). Sediment pumping by tidal asymmetry in a partially mixed estuary. *Journal of Geophysical Research*, *112*(C07028). https://doi.org/10.1029/2006jc003784

Sogreah. (2006). *Mission d'étude, d'approfondissement et d'évaluation de scénarios visant à améliorer le fonctionnement hydro seédimentaire de l'estuaire de la Loire. expertise et connaisance du système estuarien. Tome 1 - Analyse historique*. (Tech. Rep. No. 1 71 1457 R2). Author.

Sogreah. (2010). *Développement et exploitation d'un modèle hydrosédimentaire en trois dimensions sur l'estuaire de la Loire. lot 1: construction et exploitation du modèle. Phase 2: Etude et évaluation des leviers. exploitation du modèle sur l'état actuel*. (Tech. Rep. No. 1 71 1822 R10). Author.

Talke, S. A., De Swart, H. E., & De Jonge, V. N. (2009). An idealized model and systematic process study of oxygen depletion in highly turbid estuaries. *Estuaries and Coasts*, *32*(4), 602–620. https://doi.org/10.1007/s12237-009-9171-y

Van Maren, D. S., Vroom, J., Fettweis, M., & Vanlede, J. (2020). Formation of the Zeebrugge coastal turbidity maximum: The role of uncertainty in near-bed exchange processes. *Marine Geology*, *425*, 106186. https://doi.org/10.1016/j.margeo.2020.106186

Van Maren, D. S., Winterwerp, J. C., & Vroom, J. (2015). Fine sediment transport into the hyper-turbid lower Ems river: The role of channel deepening and sediment-induced drag reduction. *Ocean Dynamics*, *65*(4), 589–605. https://doi.org/10.1007/s10236-015-0821-2

Walther, R., Schaguene, J., Hamm, L., & David, E. (2012). Coupled 3d modeling of turbidity maximum dynamics in the Loire estuary, France. *Coastal Engineering Proceedings*, *1*(33), 22. https://doi.org/10.9753/icce.v33.sediment.22

Winterwerp, J. C. (2001). Stratification effects by cohesive and noncohesive sediment. *Journal of Geophysical Research*, *106*(C10), 22559–22574. https://doi.org/10.1029/2000jc000435

Winterwerp, J. C., Vroom, J., Wang, Z. B., Krebs, M., Hendriks, E. C. M., Van Maren, D. S., et al. (2017). SPM response to tide and river flow in the hyper-turbid Ems River. *Ocean Dynamics*, *67*(5), 559–583. https://doi.org/10.1007/s10236-017-1043-6

Winterwerp, J. C., & Wang, Z. B. (2013). Man-induced regime shifts in small estuaries - I: Theory. *Ocean Dynamics*, *63*(11–12), 1279–1292. https://doi.org/10.1007/s10236-013-0662-9

Winterwerp, J. C., Wang, Z. B., Van Brackel, A., Van Holland, G., & Kösters, F. (2013). Man-induced regime shifts in small estuaries - II: A comparison of rivers. *Ocean Dynamics*, *63*(11–12), 1293–1306. https://doi.org/10.1007/s10236-013-0663-8